

AbstainGNN: Teaching Graph Neural Networks to Abstain for Graph Classification

Xixun Lin
Institute of Information Engineering,
Chinese Academy of Sciences
Beijing, China
agblinxx@gmail.com

Zhiheng Zhou*
School of Mathematics and Statistics,
Shandong University
Weihai, China
zhouzhiheng@amss.ac.cn

Zhengyin Zhang
China University of Mining and
Technology-Beijing
Beijing, China
2210730330@student.cumtb.edu.cn

Yancheng Chen
Academy of Mathematics and
Systems Science, Chinese Academy of
Sciences
Beijing, China
chenyancheng22@mails.ucas.ac.cn

Shuai Zhang
Academy of Mathematics and
Systems Science, Chinese Academy of
Sciences
Beijing, China
zhangshuai2021@amss.ac.cn

Ge Zhang
School of Information and Intelligent
Science, Donghua University
Shanghai, China
gezhang@dhu.edu.cn

Shichao Zhu
TikTok, ByteDance Inc.
San Jose, United States
shichao.szhu@gmail.com

Lixin Zou
School of Cyber Science and
Engineering, Wuhan University
Wuhan, China
zoulixin@whu.edu.cn

Chuan Zhou
Academy of Mathematics and
Systems Science, Chinese Academy of
Sciences
Beijing, China
zhouchuan@amss.ac.cn

Peng Zhang
Cyberspace Institute of Advanced
Technology, Guangzhou University
Guangzhou, China
p.zhang@gzhu.edu.cn

Shirui Pan
Griffith University
Brisbane, Australia
s.pan@griffith.edu.au

Yanan Cao*
Institute of Information Engineering,
Chinese Academy of Sciences
Beijing, China
caoyanan@iie.ac.cn

Abstract

Graph classification is a core task in graph data mining with widespread real-world applications. Recent advances in graph neural networks (GNNs) have led to substantial performance improvements for graph classification. However, existing GNNs are typically forced to make predictions even under high uncertainty or unknown conditions, resulting in unreliable decisions that can severely impact downstream tasks, particularly in safety-critical scenarios. To address this critical limitation, we propose AbstainGNN, a novel and theory-driven framework for graph classification with abstention, which enables GNNs to reject uncertain predictions instead of producing incorrect decisions. Specifically, AbstainGNN explicitly models both the predictive function and the abstention

function, allowing for effective utilization of graph structural information. Moreover, unlike existing heuristic abstention methods, we theoretically characterize the trade-off between classification errors and rejection costs from a PAC-Bayesian generalization perspective, and derive a unified learning objective for model optimization. Guided by this theoretical insight, we further develop an efficient two-stage training strategy consisting of predictive function warm-start and abstention function calibration. Extensive experiments on five benchmark datasets show that AbstainGNN outperforms existing abstention methods, achieving superior classification performance under the same rejection rates.

CCS Concepts

• Computing methodologies → Machine learning; • Information systems → Data mining.

Keywords

Graph Classification, Learning with Abstention

Resource Availability:

The source code of this paper has been made publicly available at <https://doi.org/10.5281/zenodo.20422037>.

*denotes corresponding author.

Permission to make digital or hard copies of all or part of this work for personal or classroom use is granted without fee provided that copies are not made or distributed for profit or commercial advantage and that copies bear this notice and the full citation on the first page. Copyrights for components of this work owned by others than the author(s) must be honored. Abstracting with credit is permitted. To copy otherwise, or republish, to post on servers or to redistribute to lists, requires prior specific permission and/or a fee. Request permissions from permissions@acm.org.

KDD '26, Jeju Island, Republic of Korea

© 2026 Copyright held by the owner/author(s). Publication rights licensed to ACM.
ACM ISBN 978-x-xxxx-xxxx-x/YYYY/MM
<https://doi.org/10.1145/nnnnnnn.nnnnnnn>

1 Introduction

Graph classification is a fundamental task in graph data mining, which aims to assign a semantic label to an entire graph by jointly modeling graph topologies, node attributes, and edge relations [45]. Graph classification plays an important role in a wide range of real-world applications, including molecular property prediction [27, 42], material structure analysis [35, 46], and social network analysis [19, 51]. Recent advances in graph neural networks (GNNs) have substantially boosted graph classification performance. These improvements mainly stem from message passing and graph pooling mechanisms to obtain expressive graph-level representations [3, 30, 50].

Despite notable progress in graph classification, most existing GNNs still struggle to make reliable decisions. Graph samples are often forced into specific classes even when predictions are made with low confidence, ambiguous structural evidence, or weak class separation [40, 47, 49]. Such unreliable predictions can propagate severe errors to downstream tasks, compromising the trustworthiness of GNN-based decision systems [26, 28, 52]. For example, in molecular property prediction, GNNs may be compelled to classify a compound as toxic or non-toxic even when the underlying evidence is highly uncertain. Such decisions can mislead early-stage drug screening, either discarding valuable compounds or advancing risky ones into expensive evaluations. Consequently, the lack of reliable decision mechanisms significantly restricts the deployment of GNNs in high-stakes and safety-critical applications.

In fact, **Learning with Abstention**, also known as classification with rejection, provides an ideal paradigm to address the above significant limitation, enabling the model to abstain from making predictions in uncertain cases [4, 5, 9, 18, 33]. The core mechanism is to identify samples that are likely to be misclassified and defer them to human experts or downstream procedures for later decision-making. This paradigm is particularly appealing in safety-critical scenarios, where the cost of an incorrect decision can far outweigh the cost of abstention. Nevertheless, existing methods face the following two major issues in the context of graph classification:

- The majority of abstention methods have been developed for computer vision, leaving graph-structured data largely underexplored and inadequately modeled. Consequently, they fail to capture the rich topological and relational information inherent in graphs.
- Most existing methods rely heavily on heuristic model designs, offering limited theoretical insights into abstention mechanisms specifically for graphs. This lack of theoretical grounding in graph domains hinders the development of more principled and effective abstention mechanisms for graph classification.

To address these issues, we propose **AbstainGNN**, a novel abstention framework for graph classification. Specifically, AbstainGNN explicitly designs both the predictive function and the abstention function for graph-structured data, enabling more effective modeling of graph structural information. Moreover, AbstainGNN is a theory-driven learning framework rather than a heuristic model design. From the perspective of generalization bounds [32], we theoretically characterize how AbstainGNN achieves a principled trade-off between classification errors and rejection costs. This analysis leads to a unified learning objective and an efficient two-stage

learning stages, consisting of *Predictive Function Warm-start* and *Abstention Function Calibration*. In the first stage, the warm-start strategy drives the predictive function into a small-gradient region, facilitating the more stable model optimization. In the second stage, the learned predictive function is used to calibrate the abstention function, ensuring that confidence scores are well aligned with model predictions. Extensive experiments and analyses on multiple benchmark datasets demonstrate the significant advantages of our model over existing abstention methods. In general, the main contributions of our work are summarized as follows,

- **Problem Statement.** We are the first to investigate the problem of graph classification with abstention, which equips GNNs with the ability to abstain from making predictions on uncertain or unknown graph samples, significantly improving their reliability and applicability in safety-critical domains.
- **Theoretical Analysis.** We derive PAC-Bayesian generalization bounds for AbstainGNN, revealing that minimizing the intra-class variance of graph-level representations is crucial for graph classification with abstention. Building on this insight, we propose a unified learning objective for model optimization.
- **Model Implementation.** Guided by our theoretical analysis, we develop an efficient model implementation of AbstainGNN. In particular, we introduce a simple yet effective global class-cluster adjustment strategy, which alleviates the estimation bias caused by batch-wise updates.
- **Experimental Verification.** We conduct comprehensive experiments on five real-world datasets, demonstrating that our method achieves significantly superior classification performance under the same rejection rates. The most notable improvement is that our model yields an average relative risk reduction of 16.8% on MUTAG¹.

2 Related works

2.1 Graph Classification

Graph classification has been extensively studied in the data mining community. Early methods primarily rely on graph kernels, which compute the similarity between graphs based on substructures such as walks, paths, or subtrees [2, 21, 23]. While these methods are theoretically well-founded, they often require careful feature engineering and struggle to scale to large graphs. With the emergence of GNNs, graph classification has increasingly shifted toward end-to-end learning manners [11, 25, 48]. In most GNN-based methods, node representations are iteratively updated by aggregating information from their neighbors, and are subsequently pooled to produce graph-level representations. Such approaches have achieved state-of-the-art performance across a variety of applications, including drug discovery [17, 44] and protein prediction [10, 37]. Despite these advances, existing graph classification methods are typically designed to produce predictions for all input graphs, forcing the model to make decisions even on low-confidence graph samples. This design drawback introduces potential risks when deploying GNNs in high-risk and safety-critical domains.

¹Our source code is available at <https://github.com/ZZY565/AbstainGNN>.

2.2 Learning with Abstention

Learning with abstention, also known as classification with rejection, allows the classifier to refrain from making predictions on uncertain inputs, thereby reducing the risk of misclassification in critical applications [6, 20, 53]. Existing approaches can be classified broadly into two categories: cost-based and coverage-based methods. Cost-based approaches aim to prevent misclassification by providing an option not to make a prediction at the expense of the pre-defined rejection cost [4, 33, 36]. Coverage-based approaches define coverage as the proportion of samples on which the model chooses to make predictions rather than abstain. Given a coverage, the model seeks to select a subset of examples that maximizes predictive performance while rejecting the remaining uncertain samples [14–16]. Franc and Prusa [12] theoretically analyze the equivalence between these two categories. For graph domains, some works [14, 24] have followed the classic abstention mechanism to study rejection behaviors in node-level and dynamic graph scenarios. Overall, learning with abstention has primarily focused on computer vision, and how to design algorithmic and theoretical learning frameworks, especially for graph classification, remains a highly important yet largely underexplored problem.

3 Background

In this section, we describe the basic framework of GNNs for graph classification and discuss their inherent limitations under this framework. Let $G = (\mathcal{V}, \mathcal{E})$ denote an input graph, where \mathcal{V} and \mathcal{E} represent the sets of nodes and edges, respectively. The node attribute matrix is denoted by $\mathbf{X} \in \mathbb{R}^{|\mathcal{V}| \times c}$, where $|\mathcal{V}|$ is the numbers of nodes and c is the dimensionality of node attributes. The adjacency matrix is given by \mathbf{A} , where each element $\mathbf{A}_{ij} \in \{0, 1\}$ indicates whether an edge exists between nodes i and j . Graph classification aims to learn a predictive function f that maps the input graph to a probability vector $f(\mathbf{A}, \mathbf{X}) \in [0, 1]^{|\mathcal{Y}|}$, from which a predicted label is obtained. \mathcal{Y} is the set of class labels. As discussed above, GNNs have become the dominant frameworks for graph classification, which learn graph-level representations in an end-to-end manner [43].

Most GNNs can be abstracted as a composition of message-passing layers, a permutation-invariant readout operator, and a final classification layer. Formally, the entire prediction process can be written as this composite map:

$$f(\mathbf{A}, \mathbf{X}) = (C \circ R \circ U^{(L)} \circ \dots \circ U^{(1)})(\mathbf{A}, \mathbf{X}). \quad (1)$$

Here, each message-passing layer $U^{(l)}$ follows the calculation mechanism: At the l -th layer ($l = 1, \dots, L$), each node aggregates messages from its neighbors and updates its representation as follows,

$$\mathbf{m}_i^{(l)} = \sum_{j \in \mathcal{N}(i)} M^{(l)}(\mathbf{h}_i^{(l-1)}, \mathbf{h}_j^{(l-1)}, \mathbf{e}_{ij}), \quad (2)$$

$$\mathbf{h}_i^{(l)} = U^{(l)}(\mathbf{h}_i^{(l-1)}, \mathbf{m}_i^{(l)}), \quad (3)$$

where $\mathcal{N}(i)$ denotes the neighbors of the node i , $\mathbf{h}_i^{(l-1)}$ and $\mathbf{h}_j^{(l-1)}$ are the node representations of i and j in the preceding layer, and \mathbf{e}_{ij} is the (optional) edge attribute. $M^{(l)}(\cdot)$ is the message function for aggregating representations and $U^{(l)}(\cdot)$ is the update function

to generate the final representation. After L layers of propagation, a permutation-invariant readout operator is performed to obtain the graph-level representation:

$$\mathbf{h}_G = R\left(\{\mathbf{h}_i^{(L)} \mid i \in \mathcal{V}\}\right), \quad (4)$$

where $R(\cdot)$ can be the mean/sum pooling or the more sophisticated operator. Finally, a classification layer C maps \mathbf{h} to the predicted class distribution $\hat{\mathbf{y}}$:

$$\hat{\mathbf{y}} = C(\mathbf{h}_G) = \text{softmax}(\mathbf{W}\mathbf{h}_G + \mathbf{b}), \quad (5)$$

where \mathbf{W} and \mathbf{b} denote the weight matrix and the bias vector, and we denote the predicted class \hat{y} as

$$\hat{y} = \max_{y \in \mathcal{Y}} \hat{\mathbf{y}} = \max_{y \in \mathcal{Y}} f_y(\mathbf{A}, \mathbf{X}). \quad (6)$$

Current Limitation. Despite the strong performance of existing GNNs, they typically lack the ability to abstain from making predictions on unknown or out-of-distribution samples. This limitation significantly restricts their applicability, especially in risk-sensitive domains. For example, in financial risk assessment or medical diagnosis, a misclassification can lead to substantial losses or even endanger human safety, making it essential for the model to recognize when it is uncertain and avoid forced predictions. Therefore, a more desirable learning paradigm is to incorporate abstention capability into the GNN learning process, enabling GNNs to make confident predictions on reliable samples while abstaining from uncertain ones.

4 Graph Classification with Abstention

To overcome the above limitation, we introduce AbstainGNN, a novel GNN paradigm for graph classification with abstention. Let \mathcal{G} denote a space of graphs. Building upon the predictive function $f: \mathcal{G} \rightarrow [0, 1]^{|\mathcal{Y}|}$ (\mathcal{Y} is the label set), AbstainGNN introduces an additional graph-level abstention function $g: \mathcal{G} \rightarrow [0, 1]$, which determines whether a prediction should be made. Concretely, given an input graph $G = (\mathbf{A}, \mathbf{X}) \in \mathcal{G}$, AbstainGNN outputs

$$(f, g)(\mathbf{A}, \mathbf{X}) \triangleq \begin{cases} f(\mathbf{A}, \mathbf{X}), & \text{if } g(\mathbf{A}, \mathbf{X}) \geq \epsilon, \\ \text{abstain}, & \text{if } g(\mathbf{A}, \mathbf{X}) < \epsilon, \end{cases} \quad (7)$$

where ϵ is a predefined threshold. That is, AbstainGNN abstains on G if and only if the confidence score $g(\mathbf{A}, \mathbf{X})$ falls below the threshold ϵ , i.e., $g(\mathbf{A}, \mathbf{X}) < \epsilon$.

Although abstention can improve the model's accuracy, excessive abstention, where the model refrains from making predictions, renders it meaningless. Therefore, an ideal classifier with reject option should achieve a good trade-off between *coverage* and *risk* [7, 8, 18]. Given a dataset $\mathcal{S} = \{(G_i, y_i)\}_{i=1}^n \subset \mathcal{G} \times \mathcal{Y}$, the empirical coverage is defined as

$$\Phi(g \mid \mathcal{S}) \triangleq \frac{1}{n} \sum_{i=1}^n \mathbf{1}(g(\mathbf{A}_i, \mathbf{X}_i) \geq h), \quad (8)$$

which measures the fraction of graphs on which the model makes predictions. Here, $\mathbf{1}(\cdot)$ is the indicator function. The empirical risk is defined as the average loss conditioned on making predictions:

$$\Psi(f, g \mid \mathcal{S}) \triangleq \frac{\frac{1}{n} \sum_{i=1}^n \mathbf{1}(g(\mathbf{A}_i, \mathbf{X}_i) \geq h) \ell(f(\mathbf{A}_i, \mathbf{X}_i), y_i)}{\Phi(g \mid \mathcal{S})}, \quad (9)$$

where $\ell(\cdot, \cdot)$ denotes a classification loss function. Intuitively, coverage measures how often the model makes predictions, while risk quantifies the model's error on the accepted samples. Under this formulation, learning with abstention [16] aims to minimize the risk while ensuring a target coverage level c_t :

$$\min_{(f,g)} \Psi(f, g | \mathcal{S}) \quad \text{s.t.} \quad \Phi(g | \mathcal{S}) \geq c_t. \quad (10)$$

4.1 Generalization Analysis of AbstainGNN

For further analysis, we apply the Lagrangian multiplier method to Eq.(10) and derive the following per-sample reject-cost loss:

$$L(f, g; G, y) = \mathbf{1}(g(\mathbf{A}, \mathbf{X}) \geq \epsilon) \ell(f(\mathbf{A}, \mathbf{X}), y) + \lambda \mathbf{1}(g(\mathbf{A}, \mathbf{X}) < \epsilon), \quad (11)$$

where $\lambda > 0$ is the Lagrange multiplier. In Eq.(11), the first term penalizes classification errors on graphs that are *accepted* (i.e., predicted), whereas the second term assigns a fixed penalty to *rejected* graphs. By adjusting λ , we control the trade-off between minimizing the risk on accepted samples and maintaining a sufficiently high coverage to satisfy the constraint. However, the used hard indicators $\mathbf{1}(g(\mathbf{A}, \mathbf{X}) \geq \epsilon)$ and $\mathbf{1}(g(\mathbf{A}, \mathbf{X}) < \epsilon)$ make Eq.(11) non-smooth and almost everywhere non-differentiable, particularly at the boundary $g(\mathbf{A}, \mathbf{X}) = \epsilon$.

To better analyze theoretical properties of AbstainGNN, we replace Eq.(11) by a differentiable Max-Hinge loss [9]. Let $\gamma(\mathbf{A}, \mathbf{X}) = f_y(\mathbf{A}, \mathbf{X}) - \max_{j \neq y} f_j(\mathbf{A}, \mathbf{X})$ denote the classification margin of f , the margin loss is given as

$$L_{MH}^{\rho, \rho'}(f, g; G, y) = \max \left\{ \max \left[\lambda \left(1 - \beta \frac{g(\mathbf{A}, \mathbf{X})}{\rho'} \right), 0 \right], \max \left[1 + \frac{\alpha}{2} \left(\frac{g(\mathbf{A}, \mathbf{X})}{\rho'} - \frac{\gamma(\mathbf{A}, \mathbf{X})}{\rho} \right), 0 \right] \right\}, \quad (12)$$

where $\rho, \rho' > 0$ are two parameters associated with the minimum margins of f and g respectively, and $\alpha, \beta > 0$ are two balanced factors.

Let $f = C \circ R \circ U$ be an arbitrary GNN described in Section 3, where U denotes all message-passing layers, R is the pooling layer, and $C \in \mathbb{R}^{d \times |\mathcal{Y}|}$ is the classification layer (d is the dimensionality of learned graph-level representations). Let g is our proposed graph-level abstention function and $\mathcal{S} = \{(G_i, y_i)\}_{i=1}^n$ is the training dataset consisting of n i.i.d. samples drawn from an unknown data distribution \mathcal{D} , then we have the following generalization bound for AbstainGNN:

THEOREM 4.1. *For any $\rho, \rho', \alpha, \beta, \lambda > 0$, $\delta \in (0, 1)$, and $u = \max\{d, |\mathcal{Y}|\}$, with probability at least $1 - \delta$ over \mathcal{S} , it holds that*

$$\mathbb{E}_{(G, y) \sim \mathcal{D}} [L(f, g; G, y)] \leq \mathbb{E}_{(G, y) \sim \mathcal{S}} \left[L_{MH}^{\rho, \rho'}(f, g; G, y) \right] + 4 \sqrt{\frac{u \ln(4u) \left(\text{Var}_{\text{icv}}(\mathcal{S}, \mathcal{Y}) + \frac{\tilde{\rho}^2}{\|C\|_2^2} \right) + \tilde{\rho}^2 \ln\left(\frac{6u}{\delta}\right)}{(n-1)\tilde{\rho}^2}}, \quad (13)$$

where $\text{Var}_{\text{icv}}(\mathcal{S}, \mathcal{Y}) = \frac{1}{|\mathcal{Y}|} \sum_{y \in \mathcal{Y}} \frac{1}{|I_y|} \sum_{G \in I_y} \|\mathbf{h}_G - \boldsymbol{\mu}_y\|_2^2$ represents the sum of the intra-class variance of graph-level representations, I_y is a subset of \mathcal{S} that graph samples belonging to the class y , and $\boldsymbol{\mu}_y = \frac{1}{|I_y|} \sum_{G \in I_y} \mathbf{h}_G$ is the corresponding class cluster. $\|C\|_2$ denotes

the ℓ_2 -norm of model parameters of the classification layer C and $\tilde{\rho} = \min \left\{ \frac{\rho}{4\alpha}, \frac{\rho'}{4\beta\lambda + 2\alpha} \right\}$.

The detailed proof is provided in Appendix A.1. Theorem 4.1 shows that the generalization performance of AbstainGNN is upper bounded by two components: the empirical margin-based loss and the intra-class variance of graph-level representations. Therefore, reducing this intra-class variance is crucial for improving the performance of graph classification with abstention.

4.2 Learning Objective

To this end, we introduce a novel regularization loss to reduce the intra-class variance of graph-level representations:

$$\mathcal{L}_{\text{icv}} = \frac{1}{|\mathcal{Y}|} \sum_{y \in \mathcal{Y}} \sum_{G \in I_y} w_G \|\mathbf{h}_G - \boldsymbol{\mu}_y\|_2^2, \quad (14)$$

where w_G is the maximum logit of $f(\mathbf{A}, \mathbf{X})$. Based on \mathcal{L}_{icv} , the total learning objective of AbstainGNN is

$$\mathcal{L}_{\text{total}} = \mathcal{L}_{\text{ce}} + \lambda_r \mathcal{L}_{\text{icv}}, \quad (15)$$

where \mathcal{L}_{ce} is the standard cross-entropy loss for graph classification, corresponding to a smooth relaxation of the margin loss in the above generalization analysis, and λ_r is a hyper-parameter for balancing \mathcal{L}_{ce} and \mathcal{L}_{icv} . We theoretically analyze the optimization impact of $\mathcal{L}_{\text{total}}$ for $\text{Var}_{\text{icv}}(\mathcal{S}, \mathcal{Y})$:

THEOREM 4.2. *Let $\mathbf{h}_G^{(t)} \in \mathbb{R}^d$ and $\boldsymbol{\mu}_y^{(t)}$ denote the graph-level representation and the class cluster of y at the iteration t . We abbreviate $\text{Var}_{\text{icv}}(\mathcal{S}, \mathcal{Y})$ at t as $M^{(t)} = \frac{1}{|\mathcal{Y}|} \sum_{y \in \mathcal{Y}} \frac{1}{|I_y|} \sum_{G \in I_y} \|\mathbf{h}_G^{(t)} - \boldsymbol{\mu}_y^{(t)}\|_2^2$. Consider the following gradient-based updates:*

$$\mathbf{h}_G^{(t+1)} = \mathbf{h}_G^{(t)} - \eta \nabla_{\mathbf{h}_G^{(t)}} \mathcal{L}_{\text{total}}, \quad \boldsymbol{\mu}_y^{(t+1)} = \frac{1}{|I_y|} \sum_{G \in I_y} \mathbf{h}_G^{(t+1)}, \quad (16)$$

where η is the learning rate. Then $\text{Var}_{\text{icv}}(\mathcal{S}, \mathcal{Y})$ has the following one-step recursion:

$$M^{(t+1)} \leq \left(1 - \frac{4\lambda_r \eta_t}{|\mathcal{Y}| \min_y |I_y|} + \frac{12\lambda_r^2 \eta_t^2}{\max_y |I_y|^2} \right) M^{(t)} + O\left(\max_{G,t} \|\nabla_{\mathbf{h}_G^{(t)}} \mathcal{L}_{\text{ce}}\|_2^2\right) \eta. \quad (17)$$

If $0 < \eta < \delta = \min\left\{ \frac{\max_y |I_y|^2}{6|\mathcal{Y}|\lambda_r \min_y |I_y|}, \frac{|\mathcal{Y}| \min_y |I_y|}{2\lambda_r} \right\}$ and $\rho_\eta = (1 - \frac{2\lambda_r}{|\mathcal{Y}| \min_y |I_y|} \eta) \in (0, 1)$, then we have

$$M^{(t)} \leq \rho_\eta^t M^{(0)} + \frac{\eta^2}{1 - \rho_\eta} O\left(\max_{G,t} \|\nabla_{\mathbf{h}_G^{(t)}} \mathcal{L}_{\text{ce}}\|_2^2\right). \quad (18)$$

In particular, $M^{(t)}$ converges to an $O(\eta)$ -neighborhood of zero.

The detailed proof is provided in Appendix A.2. Theorem 4.2 provides an optimization-based theoretic justification for introducing \mathcal{L}_{icv} . Specifically, under the gradient descent on $\mathcal{L}_{\text{total}}$, $\text{Var}_{\text{icv}}(\mathcal{S}, \mathcal{Y})$ satisfies a contraction inequality across iterations and converges to a tighter $O(\eta)$ -neighborhood as the gradient of \mathcal{L}_{ce} diminishes during training. Consequently, minimizing \mathcal{L}_{ce} can reduce $\text{Var}_{\text{icv}}(\mathcal{S}, \mathcal{Y})$, thereby tightening the resulting generalization bound.

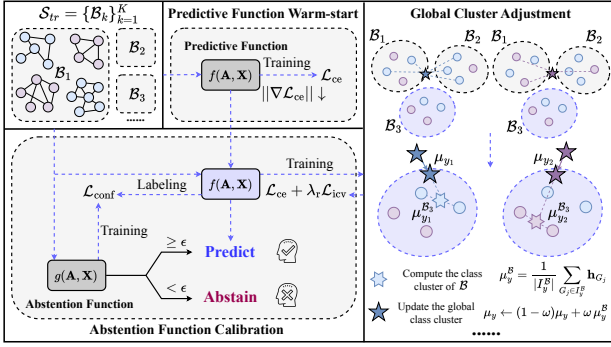


Figure 1: A simple model overview of AbstainGNN. It mainly consists of predictive function warm-start and abstention function calibration. The key operation in AbstainGNN is global cluster adjustment, which helps to more accurately estimate \mathcal{L}_{icv} .

4.3 Concrete Implementation

Based on the analyses of Theorems 4.1 and 4.2, we present a concrete implementation for optimizing the learning objective of AbstainGNN, which consists of two learning stages: *Predictive Function Warm-start* and *Abstention Function Calibration*. In the first stage, we employ a warm-start strategy for the predictive function f . Since Theorem 4.2 indicates that the reduction of $\text{Var}_{icv}(\mathcal{S}, \mathcal{Y})$ depends on the magnitude of $\|\nabla \mathcal{L}_{ce}\|$. Therefore, we first pretrain f with \mathcal{L}_{ce} to reach a small-gradient region, which accelerates the subsequent optimization of the generalization bound. In the second stage, we introduce global cluster adjustment to mitigate the estimation bias of μ_y caused by batch-wise updates. Using the learned f , we then calibrate the abstention function g so that its confidence scores are well-aligned with f 's predictions, achieving a favorable trade-off between coverage and risk for graph classification. Figure 1 shows the model overview of AbstainGNN.

Predictive Function Warm-start. Given the training dataset $\mathcal{S}_{Tr} = \{(G_i, y_i)\}_{i=1}^{|\mathcal{S}_{Tr}|} \subset \mathcal{G} \times \mathcal{Y}$, we perform a warm-start strategy using \mathcal{L}_{ce} to drive the predictive function f into a small-gradient region, yielding a stable initialization for the subsequent optimization. Following a batch-wise training manner, we first randomly shuffle \mathcal{S}_{Tr} and partition it into a collection of batches, denoted by $\mathcal{S}_{Tr} = \{\mathcal{B}_k\}_{k=1}^K$ where K is number of batches. Then, for each batch data $\mathcal{B} = \{(G_i, y_i)\}_{i=1}^{|\mathcal{B}|}$, we use the following batch-wise loss:

$$\mathcal{L}_{ce}(\mathcal{B}) = \frac{1}{|\mathcal{B}|} \sum_{i=1}^{|\mathcal{B}|} \ell_{ce}(\hat{y}_i, y_i), \quad (19)$$

where $\ell_{ce}(\cdot, \cdot)$ denotes the cross-entropy loss of the per-sample $G_i = (\mathbf{A}_i, \mathbf{X}_i)$, and $\hat{y}_i = \max_{y \in \mathcal{Y}} y f_y(\mathbf{A}_i, \mathbf{X}_i)$ denotes the predicted class of G_i . \mathcal{L}_{ce} used in Eq.(15) is the cross-entropy loss computed over all batches sampled from \mathcal{S}_{Tr} .

Abstention Function Calibration. To calculate the regularization loss in Eq.(14), we have to estimate the class cluster for each class in the representation space. A natural choice for graph classification is to estimate these class clusters via batch-wise updates. However,

such updates are often biased due to random sampling and limited batchsizes, which in turn weakens the effectiveness of the intra-class variance regularization in Eq.(14). To address this issue, we introduce *Global Cluster Adjustment* that maintains global class clusters smoothly throughout the entire training process.

Specifically, given $\mathcal{B} = \{(G_i, y_i)\}_{i=1}^{|\mathcal{B}|}$, we generate each graph-level representation \mathbf{h}_{G_i} for \mathcal{B} according to Eq.(4). For each class y , let $I_y^{\mathcal{B}} = \{G_i : y_i = y\} \subset \mathcal{B}$ that graph samples belonging to the class y . When $|I_y^{\mathcal{B}}| > 0$, the class cluster of \mathcal{B} is computed as

$$\mu_y^{\mathcal{B}} = \frac{1}{|I_y^{\mathcal{B}}|} \sum_{G_i \in I_y^{\mathcal{B}}} \mathbf{h}_{G_i}. \quad (20)$$

When $|I_y^{\mathcal{B}}| = 0$, we simply skip the update for class y in this iteration. We then update the global class cluster μ_y :

$$\mu_y \leftarrow (1 - \omega)\mu_y + \omega \mu_y^{\mathcal{B}}, \quad (21)$$

where $\omega \in (0, 1)$ is a hyper-parameter to balance the contribution of historical information and newly observed data. Through this way, $\{\mu_y\}_{y \in \mathcal{Y}}$ provides a global approximation of class clusters under the batch-wise training manner. Based on these updated clusters, we use the loss defined in Eq.(15) to optimize f .

We then train the graph-level abstention function g to predict whether the current prediction of f is correct on given graphs, thereby enabling abstention and coverage–risk evaluation. For each training sample $(G_i, y_i) \in \mathcal{B}$, we denote its predicted class as \hat{y}_i . A binary target label is introduced to indicate whether the prediction of f is correct:

$$t_i = \mathbb{I}[\hat{y}_i = y_i] \in \{0, 1\}. \quad (22)$$

This formulation cast the confidence calibration of g into a binary classification, where g is encouraged to assign high confidence scores to correctly predicted graphs and low confidence scores to misclassified ones. In AbstainGNN, g is also implemented as a GNN following the calculation process described in Eq.(1–4), the main difference is that the output of g is mapped to a scalar representing the confidence score \hat{t}_i . The batch-wise loss of \mathcal{B} for g is defined as

$$\mathcal{L}_{conf}(\mathcal{B}) = \frac{1}{|\mathcal{B}|} \sum_{(G_i, y_i) \in \mathcal{B}} \ell_{ce}(\hat{t}_i, t_i) \quad (23)$$

The total loss used to optimize g is \mathcal{L}_{conf} , which is also a cross entropy loss evaluated over all batches drawn from \mathcal{S}_{Tr} .

4.4 Computational complexity

We analyze the computational complexity of AbstainGNN. We denote by N and E the average numbers of nodes and edges in graphs within a batch, respectively. AbstainGNN follows a two-stage training framework. In the first stage, the computation is dominated by the optimization of the predictive function f , resulting in a computational complexity of $\mathcal{O}(Ed + Nd^2)$. In the second stage, the training process consists of three main components. First, computing batch-wise class clusters incurs a cost of $\mathcal{O}(|\mathcal{B}|d)$ per batch. Second, computing the regularization loss (Eq.(14)) require $\mathcal{O}(|\mathcal{B}|d)$; Third, training the graph-level abstention function g has a computational complexity of $\mathcal{O}(Ed + Nd^2)$ per iteration. Aggregating these costs, AbstainGNN maintains an acceptable computational complexity of

Table 1: Classification Error Rate (risk) at different coverage levels (%) on MUTAG, PROTEINS, and NCI1.

Coverage Method	10	30	50	70	75	80	85	90	95	Rank
	PROTEINS Classification Error Rate (%) ↓									
SR	3.4±5.1	10.7±3.0	14.5±0.7	17.9±1.1	19.6±1.7	20.7±1.6	21.7±1.3	23.5±1.1	23.9±0.9	2.8
MC-Dropout	5.2±4.3	15.2±4.7	18.8±2.3	21.3±1.6	21.4±1.5	21.6±1.8	22.2±1.6	22.1±1.7	23.0±1.6	4.6
Deep Gamblers	7.8±5.1	13.4±4.1	19.5±1.8	23.6±2.8	25.4±2.1	25.8±2.4	25.8±2.3	25.5±2.1	24.7±2.4	7.3
SAT	6.1±5.0	12.8±3.7	17.5±1.5	23.5±1.9	24.2±1.7	25.2±1.8	25.5±1.6	25.4±2.0	24.7±2.1	6.1
CCL-SC	3.5±5.1	10.4±3.0	14.8±0.7	18.2±0.3	19.5±1.2	20.3±1.6	21.4±1.4	23.4±0.8	23.7±1.1	2.7
NCwR	9.6±3.6	18.2±2.7	26.1±4.0	26.9±3.1	26.9±2.2	25.9±2.1	25.5±2.5	24.8±2.5	24.5±2.1	7.1
GraphPPD	4.5±3.2	11.0±4.6	15.4±1.8	20.1±2.1	21.0±2.1	21.5±1.9	23.2±1.1	24.5±1.1	24.7±1.3	4.4
AbstainGNN	1.8±3.6	9.5±4.1	12.9±1.2	17.4±1.0	18.2±1.0	19.3±1.3	20.5±0.6	21.7±1.0	22.7±1.2	1.0
MUTAG Classification Error Rate (%) ↓										
SR	0.0±0.0	1.7±3.7	8.4±2.9	13.8±2.1	15.7±3.2	17.3±4.4	16.3±4.0	17.1±4.0	17.8±5.4	4.1
MC-Dropout	0.0±0.0	8.3±5.3	14.7±5.2	15.4±5.4	15.0±5.2	16.7±3.7	16.9±4.2	17.6±4.6	17.2±4.8	5.6
Deep Gamblers	0.0±0.0	1.7±3.3	5.3±3.3	15.4±4.9	17.1±3.5	18.0±4.5	17.5±4.7	17.6±4.6	18.3±3.8	5.2
SAT	0.0±0.0	1.7±3.3	7.4±2.6	16.9±5.8	17.1±5.2	18.0±5.0	18.1±5.4	19.4±4.8	18.9±4.4	5.8
CCL-SC	0.0±0.0	1.7±3.3	7.4±4.2	13.1±3.1	16.4±3.6	16.7±3.7	17.5±3.8	17.1±3.4	16.7±3.9	2.9
NCwR	0.0±0.0	3.3±6.7	9.5±3.9	11.5±3.4	11.4±2.7	12.0±1.6	13.1±2.3	15.3±3.9	17.2±4.8	2.9
GraphPPD	0.0±0.0	3.6±5.0	7.4±2.9	14.8±2.7	15.0±4.7	16.7±4.7	17.5±3.6	17.6±3.6	17.8±4.6	4.2
AbstainGNN	0.0±0.0	0.0±0.0	5.2±0.1	10.4±2.7	10.7±1.5	11.5±1.8	12.5±2.1	13.3±3.2	14.8±2.7	1.0
NCI1 Classification Error Rate (%) ↓										
SR	10.6±5.2	16.1±2.2	22.5±1.3	25.8±1.4	26.9±1.5	27.9±1.7	28.6±1.4	29.5±1.3	30.2±1.6	3.7
MC-Dropout	13.7±4.1	21.1±3.2	25.4±2.8	28.2±1.7	28.5±1.6	29.3±1.6	29.7±1.7	29.9±1.6	30.5±1.8	5.9
Deep Gamblers	13.5±3.3	22.7±2.7	27.7±2.1	29.7±1.6	30.0±1.8	30.8±2.2	31.3±2.2	31.4±2.0	30.8±2.1	7.7
SAT	9.6±4.2	19.5±3.2	26.4±2.2	28.6±1.4	29.4±1.2	29.8±1.1	30.4±1.2	30.6±1.3	30.7±1.1	5.4
CCL-SC	11.1±5.1	15.6±1.6	22.4±1.1	26.4±1.7	27.4±1.5	28.2±1.3	29.0±1.4	29.6±1.3	30.3±1.5	3.6
NCwR	12.3±3.7	23.3±2.5	27.7±1.7	29.7±2.0	30.1±1.9	30.2±2.1	30.5±1.7	30.7±1.5	30.5±1.6	6.8
GraphPPD	9.5±5.5	15.3±3.1	21.3±1.2	25.2±1.5	26.5±1.3	27.2±1.5	28.0±1.3	29.0±1.1	29.9±1.1	2.0
AbstainGNN	8.5±4.1	15.1±2.4	20.9±2.1	24.2±1.5	24.9±1.6	25.7±1.5	26.8±1.8	27.6±1.4	28.4±1.6	1.0

$O((E + |\mathcal{B}|)d + Nd^2)$. An empirical comparison of training runtime is provided in 5.7.

Table 2: Statistics of used datasets.

Dataset	Graphs	Classes	Avg. nodes	Avg. edges
PROTEINS	1,113	2	39.1	72.8
MUTAG	188	2	17.9	19.8
NCI1	4,110	2	29.9	32.3
IMDB-BINARY	1,000	2	19.8	96.5
COLLAB	5,000	3	74.5	2457.8

5 Experiment

5.1 Experimental Setup

Datasets. We conduct experiments on five widely used benchmark datasets for graph classification [31], including PROTEINS, MUTAG, NCI1, IMDB-BINARY, and COLLAB. Among them, MUTAG, PROTEINS, and NCI1 are chemical graph datasets, while IMDB-BINARY and COLLAB are social graph datasets. Following previous works [1, 11], we use the provided node attributes for chemical graph datasets, where each node is represented by a one-hot encoding of its atom type. For social graph datasets, where nodes do not have inherent attributes, we adopt node degree as the

node attribute. The statistics of these datasets are summarized in Table 5.1.

We use five benchmark datasets of graph classification, and the statistics of them are provided in Table 2.

Compared Baselines. We describe compared baselines as follows,

- **SR** [15]: It is one of the most classic algorithms, which directly uses the maximum logit from the softmax layer as a confidence score to decide whether to abstain from making predictions.
- **MC-Dropout** [13]: Instead of relying on the maximum logit, this approach keeps dropout active at test time and performs multiple stochastic forward passes to estimate predictive uncertainty, which is then used as a confidence score for abstention.
- **Deep Gamblers** [29]: This method extends the original classification task by introducing an additional abstention class, enabling the model to predict the confidence of abstaining from making predictions.
- **SAT** [20]: Similar to Deep Gamblers, this method also introduces the abstention class. The key difference is that SAT can leverage model predictions during training to adaptively modulate each sample’s contribution.

Table 3: Classification Error Rate (risk) at different coverage levels (%) on IMDB-BINARY and COLLAB.

Coverage Method	10	30	50	70	75	80	85	90	95	Rank
	IMDB-BINARY Classification Error Rate (%) ↓									
SR	0.0±0.0	6.9±5.4	13.2±3.6	18.6±3.8	20.5±2.8	22.0±3.0	23.7±3.2	25.0±3.2	25.8±2.9	4.2
MC-Dropout	0.0±0.0	11.3±5.1	19.8±2.1	22.7±1.7	23.5±2.0	23.1±1.9	23.6±2.1	24.3±1.5	25.1±2.0	5.7
Deep Gamblers	<u>1.0±2.2</u>	10.9±2.0	17.4±2.4	22.0±2.2	23.0±2.3	23.6±2.5	24.2±3.0	<u>24.2±2.8</u>	<u>24.6±2.8</u>	5.6
SAT	0.0±0.0	7.2±2.3	14.7±2.7	19.7±3.3	20.8±2.8	22.4±2.0	<u>23.2±2.4</u>	24.6±3.2	25.3±2.7	4.7
CCL-SC	0.0±0.0	<u>6.9±4.8</u>	13.4±3.9	18.7±3.5	20.8±2.6	22.1±2.8	23.2±2.7	25.1±2.9	25.5±2.5	3.9
NCwR	0.0±0.0	7.2±2.3	13.8±2.9	20.1±2.4	21.5±2.2	21.8±1.6	23.8±1.4	24.3±2.2	25.1±2.3	4.6
GraphPPD	2.0±2.4	9.7±3.4	12.4±3.6	<u>18.3±3.0</u>	<u>20.1±3.7</u>	<u>21.4±3.0</u>	23.3±2.3	24.7±3.5	25.2±3.1	<u>3.6</u>
AbstainGNN	0.0±0.0	6.3±3.1	<u>13.0±3.6</u>	17.1±1.9	18.9±2.6	19.9±2.4	21.8±2.4	22.9±2.7	23.3±2.2	1.1
COLLAB Classification Error Rate (%) ↓										
SR	0.0±0.0	1.9±0.7	5.4±0.6	<u>11.6±0.7</u>	<u>13.2±0.5</u>	<u>14.6±0.4</u>	16.3±0.5	<u>17.7±0.5</u>	<u>18.8±0.4</u>	<u>2.2</u>
MC-Dropout	0.0±0.0	1.5±0.5	8.5±0.3	15.5±0.5	16.6±0.4	17.6±0.7	18.4±0.7	19.1±0.8	19.7±0.6	6.0
Deep Gamblers	0.0±0.0	4.7±1.8	9.3±0.8	12.7±1.0	13.9±0.9	15.3±1.1	16.7±0.8	17.8±0.7	19.2±0.7	4.7
SAT	0.0±0.0	2.8±1.3	6.5±1.6	12.7±1.0	14.5±0.9	16.0±0.8	17.2±0.8	18.4±0.7	19.5±0.6	5.4
CCL-SC	0.0±0.0	2.1±0.5	6.0±1.3	11.8±1.2	13.4±1.3	15.1±1.1	16.6±0.8	17.8±0.7	19.3±0.9	3.2
NCwR	<u>5.8±2.0</u>	10.5±3.4	14.1±3.0	16.7±1.8	17.3±1.4	17.9±1.3	18.5±0.9	18.9±0.7	19.3±0.5	6.9
GraphPPD	0.0±0.0	<u>1.5±0.3</u>	<u>4.8±0.7</u>	12.2±0.6	13.8±0.4	15.6±0.7	16.7±0.6	18.2±0.6	19.5±0.7	3.6
AbstainGNN	0.0±0.0	1.4±0.4	4.0±0.7	10.8±0.8	12.1±0.5	13.9±0.8	15.7±0.4	17.4±0.5	18.0±0.4	1.0

- **CCL-SC** [41]: It is a competitive coverage-based method that leverages contrastive learning to aggregate the representations of samples in the same category, leading to improved performance under coverage constraints.
- **NCwR** [24]: This is the first work that introduces abstention into node classification. It proposes both cost-based and coverage-based formulations, and we adopt the cost-based variant due to its superior empirical performance.
- **GraphPPD** [34]: It proposes a variational modeling framework to estimate the uncertainty as the rejection criterion.

Implementation Details. Since the first six baselines are not designed for graph-level tasks, we adopt the same GNN backbone as the predictive function for both our model and these baselines, following the optimal hyper-parameter settings reported in their original literature. For GraphPPD, we reproduce its proposed feature extractor and posterior approximation as described in the original paper. In our model, the predictive function f is implemented using a simple GNN architecture consisting of 3 GCNConv layers [22] as message-passing layers, with sum pooling as the readout operator. The graph-level abstention function g shares the same GNN framework as f , except that it contains only 1 GCNConv layer. For all datasets, the training–testing split ratio is fixed at 0.8:0.2. We conduct experiments with five different random seeds and report the mean and variance of empirical results.

To ensure a fair comparison, the dimensionality of the learned graph-level representations is fixed to 64 for all methods. The balanced factor ω in Eq.(21) is fixed as 0.5. We use grid search to tune the remaining hyper-parameters. The search spaces are given here: λ_r in Eq.(15) $\in \{0.1, 0.3, 0.5, 0.7, 0.9\}$, the number of warm-start epochs $T_{ws} \in \{50, 100, 150, 175, 200\}$, and the batchsize $|\mathcal{B}| \in \{16, 32, 64, 128, 256\}$. In addition, the number of epochs in the second stage is fixed to 50, and an early stopping strategy is applied.

Model training is terminated when the sum of the losses of f and g no longer decrease for three consecutive epochs.

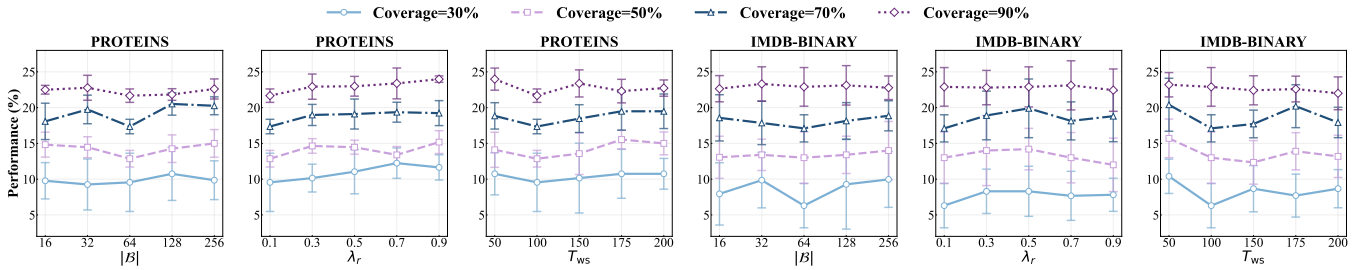
Metrics. In classification with rejection, two key quantities are coverage and risk. Following the standard evaluation protocol [4, 15, 16], we first rank all test samples using the abstention function and then select the top-ranked samples for prediction at different coverage levels. Specifically, the coverage levels are varied from $\{10\%, 30\%, 50\%, 70\%, 75\%, 80\%, 85\%, 90\%, 95\%\}$. This design choice is motivated by the fact that, at low coverage levels, most methods can easily select high-confidence samples, which does not accurately reflect the true model capability. Therefore, we adopt a finer-grained partition at higher coverage levels. Risk is evaluated by the classification error rate.

5.2 Performance Comparison

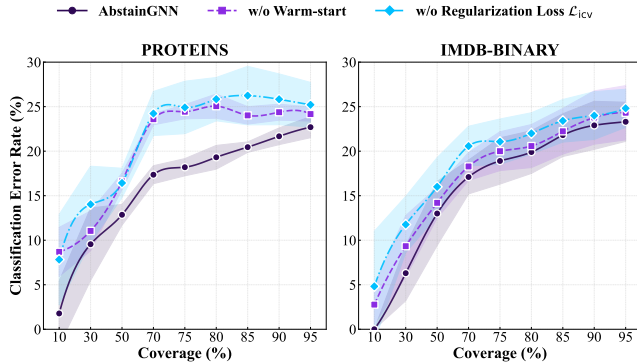
Table 1 and Table 3 report the risk comparison under different coverage levels on chemical graph datasets and social graph datasets, respectively. The best and second-best results are highlighted in bold and underlined. From these results, we can draw the following conclusions. (1) Across all datasets, AbstainGNN demonstrates clear improvements across different coverage levels. In particular, AbstainGNN yields an average relative risk reduction of 9.8% on PROTEINS, 16.8% on MUTAG, 4.8% on NCI1, 15.8% on IMDB-BINARY, and 5.9% on COLLAB. (2) At low coverage levels, high-confidence samples are relatively easy to identify. As a result, on MUTAG, IMDB-BINARY, and COLLAB, many methods achieve zero risk when the coverage is set to 10%. However, as the coverage increases, especially beyond 80%, our method is still able to select reliable decision samples, leading to consistently superior performance. (3) The baselines show large performance discrepancies for different datasets. For instance, NCwR achieves competitive results on MUTAG, but performs moderately on social graph datasets.

Table 4: Performance Comparisons of different model variants of AbstainGNN on PROTEINS and IMDB-BINARY.

Method	Coverage									
	10	30	50	70	75	80	85	90	95	
PROTEINS Classification Error Rate (%) ↓										
AbstainGNN-GAT	4.5±4.5	9.2±4.6	15.3±2.2	21.5±2.2	21.8±2.2	21.7±2.0	22.1±1.8	22.3±1.8	22.5±2.0	
AbstainGNN-MLP	7.1±6.0	12.2±4.9	18.0±1.6	24.4±2.3	25.2±2.4	25.5±2.0	25.7±1.9	25.7±2.2	25.0±2.0	
AbstainGNN-BC	6.1±6.6	12.5±5.1	17.7±3.3	23.2±2.7	23.8±2.7	24.3±2.4	24.3±3.0	24.4±2.9	24.1±3.1	
AbstainGNN	1.8±3.6	9.5±4.1	12.9±1.2	17.4±1.0	18.2±1.0	19.3±1.3	20.5±0.6	21.7±1.0	22.7±1.2	
IMDB-BINARY Classification Error Rate (%) ↓										
AbstainGNN-GAT	3.0±2.5	11.7±3.0	15.0±1.8	19.3±2.1	20.5±2.6	21.6±3.3	23.1±2.9	23.6±3.1	24.4±2.9	
AbstainGNN-MLP	8.4±3.8	16.9±3.2	21.4±4.2	23.9±3.7	24.1±2.9	24.6±2.0	24.9±2.1	25.9±1.7	26.6±1.8	
AbstainGNN-BC	3.0±4.0	11.3±3.7	16.6±2.6	20.9±2.5	22.0±2.4	22.8±2.5	23.5±1.6	23.9±2.4	25.3±1.6	
AbstainGNN	0.0±0.0	6.3±3.1	13.0±3.6	17.1±1.9	18.9±2.6	19.9±2.4	21.8±2.4	22.9±2.7	23.3±2.2	

**Figure 2: Hyperparameter Sensitivity Analysis of AbstainGNN.**

Compared with these baselines, our model exhibits superior generalization and consistently achieves the best overall performance across all datasets.

**Figure 3: Ablation Study of AbstainGNN.**

5.3 Ablation Study

Figure 3 presents an ablation study of AbstainGNN on PROTEINS and IMDB-BINARY across different coverage levels. ‘w/o Warm-start’ refers to the one that removes the first stage of predictive function warm-start and only performs the second stage of abstention function calibration. ‘w/o Regularization Loss \mathcal{L}_{icv} ’ denotes the one that excludes the intra-class variance regularization in

Eq.(14), optimizing f and g solely with the cross-entropy loss. As shown in Figure 3, removing either component consistently degrades the risk–coverage trade-off, with the gap becoming more obvious at medium-to-high coverage levels. On PROTEINS, AbstainGNN achieves the lowest risk across all coverages, and its advantage grows substantially once the coverage exceeds 50%. On IMDB-BINARY, we observe a similar but relatively milder trend. Overall, these results confirm the benefits of warm-start and \mathcal{L}_{icv} : warm-start stabilizes the optimization process, while \mathcal{L}_{icv} strengthens the regularization of graph-level representations, which is particularly important at higher coverage levels.

5.4 Model Variants

In this section, we design three model variants: AbstainGNN-GAT, AbstainGNN-MLP, and AbstainGNN-BC. AbstainGNN-GAT replaces GCNConv layers with graph attention networks (GAT) [39] to model the abstention function g . AbstainGNN-MLP employs a multilayer perceptron (MLP) to model g , ignoring graph structural information. AbstainGNN-BC removes global cluster adjustment and instead relies on batch-wise class clusters to optimize f . Table 4 reports their comparisons on PROTEINS and IMDB-BINARY. From the results, we make the following observations. (1) AbstainGNN-MLP performs substantially worse than both AbstainGNN-GAT and AbstainGNN, indicating that the ability of g to capture graph structural information is crucial. Although AbstainGNN-GAT slightly outperforms AbstainGNN on a few coverage levels on PROTEINS, AbstainGNN achieves the best overall performance. In addition, AbstainGNN-GAT incurs higher computational complexity than

AbstainGNN, suggesting that designing more suitable GNN architectures for g is a promising direction for future work. (2) Compared with AbstainGNN-BC, AbstainGNN consistently achieves superior results, showing that optimizing \mathcal{L}_{icv} based on batch-wise class clusters is insufficient. Maintaining global class clusters, as adopted in AbstainGNN, is a more effective strategy.

5.5 Hyper-parameter Analysis

Figure 2 analyzes the impact of three main hyper-parameters: λ_r , T_{ws} , and $|\mathcal{B}|$, as described in Section 5.1. Several observations can be drawn from this figure. (1) Setting $\lambda_r = 0.1$ leads to the best overall performance. This choice effectively reduces intra-class variance to improve confidence ranking, while avoiding overly compact graph-level representations that would reduce effective margins and degrade performance at high coverage levels. (2) The optimal warm-start epoch is $T_{ws} = 100$. This warm-start strategy aims to reduce the magnitude of the cross-entropy gradients. After sufficient warm-up, the updates of \mathcal{L}_{ce} become more stable, enabling \mathcal{L}_{icv} to be effectively optimized. (3) A batchsize of $|\mathcal{B}| = 64$ achieves the best trade-off between model performance and training stability. The small batchsizes yield noisy estimates of the batch-wise class clusters, and an excessively large batchsize can adversely affect the optimization process, potentially causing convergence issues.

5.6 Visual Analysis

We present a visual analysis of how the proposed regularization term, \mathcal{L}_{icv} , reduces the intra-class variance of graph-level representations. Figure 4 illustrates the class-wise intra-class variance during training on PROTEINS and IMDB-BINARY. During the warm-start stage, the variance remains relatively high and changes only slightly, as optimization is primarily driven by the standard cross-entropy loss. However, once the training transitions to the second stage at epoch 100, the variance sharply decreases for both classes on both datasets and continues to decline in subsequent epochs. The emergence of this distinct inflection suggests that \mathcal{L}_{icv} encourages graph-level representations to concentrate within tighter class clusters, thereby reducing the intra-class variance.

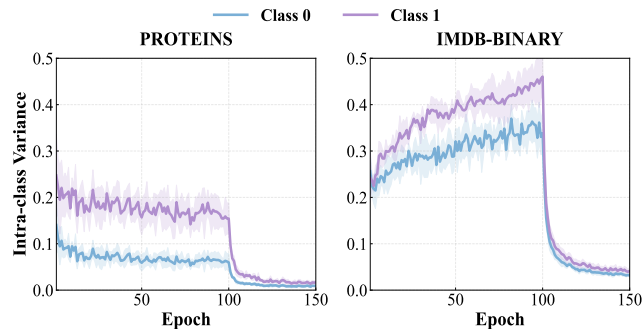


Figure 4: Visual analysis of intra-class variance curves.

5.7 Runtime Comparison

We empirically compare the runtime of our model with that of competing baselines in terms of per-epoch training time. Experiments are conducted on PROTEINS and IMDB-BINARY under the same training setting. Figure 5 reports the average training time of a single epoch. The results show that AbstainGNN incurs only a moderate computational overhead compared to all baselines, while remaining within an acceptable runtime range. This indicates that the proposed two-stage training strategy introduces limited additional cost, achieving a favorable balance between model effectiveness and computational efficiency.

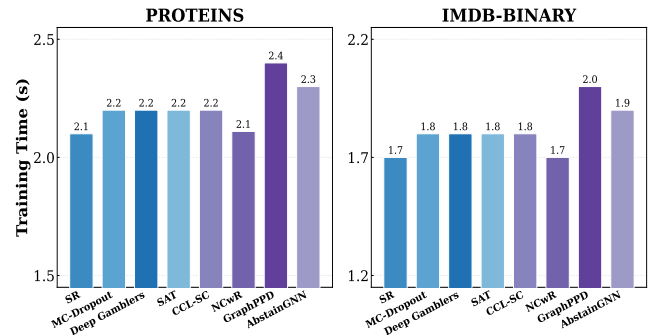


Figure 5: Per-epoch training time comparison.

6 Conclusion

In this paper, we propose AbstainGNN which explicitly equips GNNs with the ability to abstain from making predictions when confidence is insufficient. We provide a rigorous theoretical analysis of AbstainGNN from the perspectives of generalization bounds and training convergence. Guided by these theoretical insights, we further develop an efficient implementation of the proposed framework, including the predictive function warm-start to stabilize loss optimization and the abstention function calibration to ensure well-behaved abstention decisions. We conduct experiments on five benchmark datasets of graph classification. Extensive empirical results and analyses validate both the effectiveness of model designs and the soundness of theoretical derivations. In the future, we plan to extend the proposed abstention mechanism to a wider range of graph-related tasks and explore more suitable model architectures for AbstainGNN.

Acknowledgments

This work is supported by the National Natural Science Foundation of China (No.62402491, No.U2336202, No.62472416, No.62376064, U23A20305, and 62302345), and is also supported by Shanghai Pujiang Program (No.24PJA004). We thank the reviewers for their thoughtful feedback and constructive suggestions, which have helped us substantially improve the manuscript.

References

- [1] Cristian Bodnar, Fabrizio Frasca, Yuguang Wang, Nina Otter, Guido F Montufar, Pietro Lio, and Michael Bronstein. 2021. Weisfeiler and Lehman go topological: Message passing simplicial networks. In *International conference on machine learning*. PMLR, 1026–1037.
- [2] Karsten Borgwardt and Hans-Peter Kriegel. 2005. Protein function prediction via graph kernels. In *ISMB*.
- [3] David Buterez, Jon Paul Janet, Dino Oglic, and Pietro Liò. 2025. An end-to-end attention-based approach for learning on graphs. *Nature Communications* 16, 1 (2025), 5244.
- [4] Nontawat Charoenphakdee, Zhenghang Cui, Yivan Zhang, and Masashi Sugiyama. 2021. Classification with rejection based on cost-sensitive classification. In *International Conference on Machine Learning*. PMLR, 1507–1517.
- [5] C Chow. 1970. On optimum recognition error and reject tradeoff. *IEEE Transactions on Information Theory* (1970).
- [6] C Chow. 2003. On optimum recognition error and reject tradeoff. *IEEE Transactions on information theory* 16, 1 (2003), 41–46.
- [7] C. K. Chow. 1970. On optimum recognition error and reject tradeoff. *IEEE Transactions on Information Theory* 16, 1 (1970), 41–46.
- [8] Corinna Cortes, Giulia DeSalvo, and Mehryar Mohri. 2016. Boosting with abstention. *Advances in neural information processing systems* 29 (2016).
- [9] Corinna Cortes, Giulia DeSalvo, and Mehryar Mohri. 2016. Learning with rejection. *Journal of Machine Learning Research* 17, 130 (2016), 1–19.
- [10] Paul Dobson and Andrew Doig. 2003. Predicting protein function from structure. *Molecular BioSystems* (2003).
- [11] Federico Errica, Marco Podda, Davide Bacciu, and Alessio Micheli. 2019. A fair comparison of graph neural networks for graph classification. *arXiv preprint arXiv:1912.09893* (2019).
- [12] Vojtech Franc and Daniel Prusa. 2019. On discriminative learning of prediction uncertainty. In *International conference on machine learning*. PMLR, 1963–1971.
- [13] Yarin Gal and Zoubin Ghahramani. 2016. Dropout as a Bayesian Approximation: Representing Model Uncertainty in Deep Learning. In *Proceedings of the 33rd International Conference on Machine Learning*. PMLR, 1050–1059.
- [14] Jayadratha Gayen, Himanshu Pal, Naresh Manwani, and Charu Sharma. 2025. Predict Confidently, Predict Right: Abstention in Dynamic Graph Learning. *arXiv preprint arXiv:2501.08397* (2025).
- [15] Yonatan Geifman and Ran El-Yaniv. 2017. Selective classification for deep neural networks. *Advances in neural information processing systems* 30 (2017).
- [16] Yonatan Geifman and Ran El-Yaniv. 2019. Selectivenet: A deep neural network with an integrated reject option. In *International conference on machine learning*. PMLR, 2151–2159.
- [17] Justin Gilmer, Samuel S Schoenholz, Patrick F Riley, Oriol Vinyals, and George E Dahl. 2017. Neural message passing for quantum chemistry. In *International conference on machine learning*. PMLR, 1263–1272.
- [18] Yves Grandvalet, Alain Rakotomamonjy, Joseph Keshet, and Stéphane Canu. 2008. Support vector machines with a reject option. *Advances in neural information processing systems* 21 (2008).
- [19] Mei Guo, Chen Chen, Chunyan Hou, Yike Wu, and Xiaojie Yuan. 2025. FGDGNN: Fine-Grained Dynamic Graph Neural Network for Rumor Detection on Social Media. In *Findings of the Association for Computational Linguistics: ACL 2025*. 5676–5687.
- [20] Lang Huang, Chao Zhang, and Hongyang Zhang. 2020. Self-adaptive training: beyond empirical risk minimization. *Advances in neural information processing systems* 33 (2020), 19365–19376.
- [21] Hisashi Kashima, Koji Tsuda, and Akihiro Inokuchi. 2003. Marginalized kernels between labeled graphs. In *Proceedings of the 20th international conference on machine learning (ICML-03)*. 321–328.
- [22] Thomas Kipf and Max Welling. 2016. Semi-supervised classification with graph convolutional networks.
- [23] Nils Kriege, Fredrik Johansson, and Christopher Morris. 2020. A survey on graph kernels. *Applied Network Science* (2020).
- [24] Uday Bhaskar Kuchipudi, Jayadratha Gayen, Charu Sharma, and Naresh Manwani. 2025. Node Classification With Reject Option. *Transactions on Machine Learning Research* (2025).
- [25] Zhi-Peng Li, Si-Guo Wang, Qin-Hu Zhang, Yi-Jie Pan, Nai-An Xiao, Jia-Yang Guo, Chang-An Yuan, Wen-Jian Liu, and De-Shuang Huang. 2024. Graph pooling for graph-level representation learning: a survey. *Artificial Intelligence Review* 58, 2 (2024), 45.
- [26] Xixun Lin, Yanan Cao, Nan Sun, Lixin Zou, Chuan Zhou, Peng Zhang, Shuai Zhang, Ge Zhang, and Jia Wu. 2025. Conformal graph-level out-of-distribution detection with adaptive data augmentation. In *Proceedings of the ACM on Web Conference 2025*. 4755–4765.
- [27] Xixun Lin, Zhao Li, Peng Zhang, Luchen Liu, Chuan Zhou, Bin Wang, and Zhihong Tian. 2022. Structure-aware prototypical neural process for few-shot graph classification. *IEEE Transactions on Neural Networks and Learning Systems* 35, 4 (2022), 4607–4621.
- [28] Xixun Lin, Qing Yu, Yanan Cao, Lixin Zou, Chuan Zhou, Jia Wu, Chenliang Li, Peng Zhang, and Shirui Pan. 2025. Generative Causality-driven Network for Graph Multi-task Learning. *IEEE transactions on pattern analysis and machine intelligence* (2025).
- [29] Ziyin Liu, Zhikang Wang, Paul Pu Liang, Russ R Salakhutdinov, Louis-Philippe Morency, and Masahito Ueda. 2019. Deep gamblers: Learning to abstain with portfolio theory. *Advances in Neural Information Processing Systems* 32 (2019).
- [30] Diego Mesquita, Amauri Souza, and Samuel Kaski. 2020. Rethinking pooling in graph neural networks. *Advances in Neural Information Processing Systems* 33 (2020), 2220–2231.
- [31] Christopher Morris, Nils M Kriege, Franka Bause, Kristian Kersting, Petra Mutzel, and Marion Neumann. 2020. Tudataset: A collection of benchmark datasets for learning with graphs. *arXiv preprint arXiv:2007.08663* (2020).
- [32] Behnam Neyshabur, Srinadh Bhojanapalli, and Nathan Srebro. 2017. A pac-bayesian approach to spectrally-normalized margin bounds for neural networks. *arXiv preprint arXiv:1707.09564* (2017).
- [33] Chenri Ni, Nontawat Charoenphakdee, Junya Honda, and Masashi Sugiyama. 2019. On the calibration of multiclass classification with rejection. *Advances in neural information processing systems* 32 (2019).
- [34] Soumyasundar Pal, Liheng Ma, Amine Natick, Yingxue Zhang, and Mark Coates. 2025. GraphPPD: Posterior Predictive Modelling for Graph-Level Inference. *arXiv preprint arXiv:2508.16995* (2025).
- [35] Cheol Woo Park and Chris Wolverton. 2020. Developing an improved crystal graph convolutional neural network framework for accelerated materials discovery. *Physical Review Materials* 4, 6 (2020), 063801.
- [36] Harish G Ramaswamy, Ambuj Tewari, and Shivani Agarwal. 2018. Consistent algorithms for multiclass classification with an abstain option. (2018).
- [37] Nino Shervashidze, Pascal Schweitzer, Erik Van Leeuwen, Kurt Mehlhorn, and Karsten Borgwardt. 2011. Weisfeiler-Lehman graph kernels. In *NeurIPS*.
- [38] Joel A Tropp. 2012. User-friendly tail bounds for sums of random matrices. *Foundations of computational mathematics* 12, 4 (2012), 389–434.
- [39] Petar Veličković, Guillem Cucurull, Arantxa Casanova, Adriana Romero, Pietro Lio, and Yoshua Bengio. 2017. Graph attention networks. *arXiv preprint arXiv:1710.10903* (2017).
- [40] Bingzhe Wu, Yatao Bian, Hengtong Zhang, Jintang Li, Junchi Yu, Liang Chen, Chaohao Chen, and Junzhou Huang. 2022. Trustworthy graph learning: Reliability, explainability, and privacy protection. In *Proceedings of the 28th ACM SIGKDD conference on knowledge discovery and data mining*. 4838–4839.
- [41] Yu-Chang Wu, Shen-Huan Lyu, Haopu Shang, Xiangyu Wang, and Chao Qian. 2024. Confidence-aware Contrastive Learning for Selective Classification. In *ICML*.
- [42] Zonghan Wu, Shirui Pan, Fengwen Chen, Guodong Long, Chengqi Zhang, and Philip S Yu. 2020. A comprehensive survey on graph neural networks. *IEEE transactions on neural networks and learning systems* 32, 1 (2020), 4–24.
- [43] Zonghan Wu, Shirui Pan, Fengwen Chen, Guodong Long, Chengqi Zhang, and Philip S. Yu. 2021. A comprehensive survey on graph neural networks. *IEEE Transactions on Neural Networks and Learning Systems* 32, 1 (2021), 4–24. doi:10.1109/TNNLS.2020.2978386
- [44] Zhenqin Wu, Bharath Ramsundar, Evan Feinberg, Joseph Gomes, et al. 2018. MoleculeNet: A benchmark for molecular machine learning. *Chemical Science* (2018).
- [45] Feng Xia, Ke Sun, Shuo Yu, Abdul Aziz, Liangtian Wan, Shirui Pan, and Huan Liu. 2021. Graph learning: A survey. *IEEE Transactions on Artificial Intelligence* 2, 2 (2021), 109–127.
- [46] Tian Xie and Jeffrey C Grossman. 2018. Crystal graph convolutional neural networks for an accurate and interpretable prediction of material properties. *Physical review letters* 120, 14 (2018), 145301.
- [47] Xiaotian Xie, Biao Luo, Yingjie Li, Chunhua Yang, and Weihua Gui. 2024. Exploring heterophily in calibration of graph neural networks. *Neurocomputing* 604 (2024), 128294.
- [48] Keyulu Xu, Weihua Hu, Jure Leskovec, and Stefanie Jegelka. 2018. How powerful are graph neural networks? *arXiv preprint arXiv:1810.00826* (2018).
- [49] Hao Yang, Min Wang, Qi Wang, Mingrui Lao, and Yun Zhou. 2024. Balanced confidence calibration for graph neural networks. In *Proceedings of the 30th ACM SIGKDD Conference on Knowledge Discovery and Data Mining*. 3747–3757.
- [50] Chaolong Ying, Xinjian Zhao, and Tianshu Yu. 2024. Boosting graph pooling with persistent homology. *Advances in Neural Information Processing Systems* 37 (2024), 19087–19113.
- [51] Zhitao Ying, Jiaxuan You, Christopher Morris, Xiang Ren, Will Hamilton, and Jure Leskovec. 2018. Hierarchical graph representation learning with differentiable pooling. *Advances in neural information processing systems* 31 (2018).
- [52] He Zhang, Bang Wu, Xingliang Yuan, Shirui Pan, Hanghang Tong, and Jian Pei. 2024. Trustworthy graph neural networks: Aspects, methods, and trends. *Proc. IEEE* 112, 2 (2024), 97–139.
- [53] Yinglun Zhu and Robert Nowak. 2022. Efficient active learning with abstention. *Advances in Neural Information Processing Systems* 35 (2022), 35379–35391.

A Appendix

A.1 Proof of Theorem 4.1

We first establish an intermediate lemma that converts the abstention objective into an empirical margin-based loss with a complexity term measured.

LEMMA A.1. *Let $f_w : \mathcal{G} \rightarrow [0, 1]^{|\mathcal{Y}|}$ be any predictive function parameterized by w in Section 4 and P be any prior distribution over the model parameters that is independent of the training sample \mathcal{S} . Fix $\rho, \rho', \alpha, \beta, \lambda > 0$ and $\delta \in (0, 1)$. Then, with probability at least $1 - \delta$ over the draw of a training dataset \mathcal{S} consisting of n i.i.d. graph samples from the data distribution \mathcal{D} , the following inequality holds for any w and any random perturbation u simultaneously:*

$$\mathbb{P}_u \left[\max_{(G, y) \in \mathcal{S}} \|f_{w+u}(\mathbf{A}, \mathbf{X}) - f_w(\mathbf{A}, \mathbf{X})\|_2 < \min \left\{ \frac{\rho}{4\alpha}, \frac{\rho'}{4\beta\lambda + 2\alpha} \right\} \right] \geq \frac{1}{2}. \quad (24)$$

Under this condition, we have

$$\begin{aligned} \mathbb{E}_{(G, y) \sim \mathcal{D}} [L(f, g; G, y)] &\leq \mathbb{E}_{(G, y) \sim \mathcal{S}} \left[L_{MH}^{\rho, \rho'}(f, g; G, y) \right] \\ &\quad + 4 \sqrt{\frac{\text{KL}(w + u \| P) + \ln(\frac{6n}{\delta})}{n-1}}, \end{aligned} \quad (25)$$

where $\text{KL}(w + u \| P)$ denotes the KL divergence.

PROOF. Let $w' = w + u$ and $\tilde{\rho} = \min \left\{ \frac{\rho}{4\alpha}, \frac{\rho'}{4\beta\lambda + 2\alpha} \right\}$, we define

$$S_w = \left\{ w' : \max_{(G, y) \in \mathcal{S}} \|f_{w'}(\mathbf{A}, \mathbf{X}) - f_w(\mathbf{A}, \mathbf{X})\|_2 < \tilde{\rho} \right\}, \quad (26)$$

By assumption, $Z = \mathbb{P}_u[w + u \in S_w] \geq \frac{1}{2}$. Let \tilde{Q} denote the conditional distribution of $w' \in S_w$, and we denote the weight sample $\tilde{w} \sim \tilde{Q}$ and $\tilde{w} \in S_w$ almost surely. Fix any graph-label pair (G, y) , and let $p_w(G) = f_w(\mathbf{A}, \mathbf{X})$. For any $i, j \in \mathcal{Y}$, we have

$$\begin{aligned} &| (p_{\tilde{w}}(G)[i] - p_{\tilde{w}}(G)[j]) - (p_w(G)[i] - p_w(G)[j]) | \\ &\leq |p_{\tilde{w}}(G)[i] - p_w(G)[i]| + |p_{\tilde{w}}(G)[j] - p_w(G)[j]| \\ &\leq 2\|p_{\tilde{w}}(G) - p_w(G)\|_2 < 2\tilde{\rho}. \end{aligned} \quad (27)$$

Let the margin be $\gamma_w(G, y) = p_w(G)[y] - \max_{j \neq y} p_w(G)[j]$. Then the above bound implies $|\gamma_{\tilde{w}}(G, y) - \gamma_w(G, y)| < 2\tilde{\rho} \leq \frac{\rho'}{2\alpha}$.

We denote the graph-level abstention score $g_w(\mathbf{A}, \mathbf{X}) = g_w(G)$ associated with the model parameters w , and assume it is 1-Lipschitz with respect to $p_w(G)$ under $\|\cdot\|_2$, then

$$|g_{\tilde{w}}(G) - g_w(G)| \leq \|p_{\tilde{w}}(G) - p_w(G)\|_2 < \tilde{\rho} \leq \frac{\rho'}{4\beta\lambda + 2\alpha}. \quad (28)$$

We define the ‘‘halved-margin’’ loss $L_{MH}^{\rho/2, \rho'/2}$ by replacing (ρ, ρ') in $L_{MH}^{\rho, \rho'}$ with $(\rho/2, \rho'/2)$ as follows,

$$\begin{aligned} \mathbb{E}_{(G, y) \sim \mathcal{D}} \left[L_{MH}^{\rho/2, \rho'/2}(f, g; G, y) \right] &= \mathbb{P}_{\mathcal{D}}[p(G) \leq \frac{\rho}{2\alpha}] \\ \mathbb{P}_{\mathcal{D}}[g(G) > -\frac{\rho'}{4\beta\lambda + 2\alpha}] + \lambda \mathbb{P}_{\mathcal{D}}[g(G) > \frac{\rho'}{4\beta\lambda + 2\alpha}]. \end{aligned} \quad (29)$$

Using the margin controls and the monotonicity of the hinge terms in $L_{MH}^{\rho, \rho'}$, we obtain the following comparisons:

$$\begin{aligned} \mathbb{E}_{(G, y) \sim \mathcal{D}} [L(f_w, g_w; G, y)] &\leq \mathbb{E}_{(G, y) \sim \mathcal{D}} \left[L_{MH}^{\rho/2, \rho'/2}(f_w, g_w; G, y) \right], \\ \mathbb{E}_{(G, y) \sim \mathcal{S}} \left[L_{MH}^{\rho/2, \rho'/2}(f_w, g_w; G, y) \right] &\leq \mathbb{E}_{(G, y) \sim \mathcal{S}} \left[L_{MH}^{\rho, \rho'}(f_w, g_w; G, y) \right]. \end{aligned} \quad (30)$$

Applying the PAC-Bayesian bound [32] to the loss $L_{MH}^{\rho/2, \rho'/2}$, the prior distribution P , and the conditional distribution \tilde{Q} , with the probability at least $1 - \delta$ over \mathcal{S} , we have

$$\begin{aligned} \mathbb{E}_{(G, y) \sim \mathcal{D}} \left[L_{MH}^{\rho/2, \rho'/2}(f_w, g_w; G, y) \right] &\leq \mathbb{E}_{(G, y) \sim \mathcal{S}} \left[L_{MH}^{\rho/2, \rho'/2}(f_w, g_w; G, y) \right] \\ &\quad + 2\sqrt{\frac{2\text{KL}(\tilde{Q} \| P) + \ln(\frac{2n}{\delta})}{n-1}}. \end{aligned} \quad (31)$$

Since \tilde{Q} is the distribution of w' conditioned on $\{w' \in S_w\}$, a standard condition inequality gives

$$\text{KL}(\tilde{Q} \| P) \leq \text{KL}(w + u \| P) + \ln\left(\frac{1}{Z}\right) \leq \text{KL}(w + u \| P) + \ln 2. \quad (32)$$

The second inequality holds because $Z \geq 1/2$. Absorbing constants into the logarithmic term and using $\sqrt{2(a+b)} \leq \sqrt{2a} + \sqrt{2b}$ followed by a coarse simplification, we yield

$$2\sqrt{\frac{2\text{KL}(\tilde{Q} \| P) + \ln(\frac{2n}{\delta})}{n-1}} \leq 4\sqrt{\frac{\text{KL}(w + u \| P) + \ln(\frac{6n}{\delta})}{n-1}}. \quad (33)$$

Then, we have

$$\begin{aligned} \mathbb{E}_{(G, y) \sim \mathcal{D}} [L(f_w, g_w; G, y)] &\leq \mathbb{E}_{(G, y) \sim \mathcal{S}} \left[L_{MH}^{\rho, \rho'}(f_w, g_w; G, y) \right] \\ &\quad + 4\sqrt{\frac{\text{KL}(w + u \| P) + \ln(\frac{6n}{\delta})}{n-1}}. \end{aligned} \quad (34)$$

□

PROOF OF THEOREM 4.1. With Lemma A.1, we focus on bounding the KL divergence term $\text{KL}(w + u \| P)$ to derive Theorem 4.1. Let $C_w^e \in \mathbb{R}^{d \times |\mathcal{Y}|}$ be a random matrix with independent entries that have a mean of 0 and a variance of σ^2 . We can derive a perturbed predictive function f^e by replacing the weight parameters C_w of the classification layer C with $C_w + C_w^e$. We write $u = \max\{d, |\mathcal{Y}|\}$ for convenience. Through a standard tail bound for Gaussian random matrices [38], for any $t \geq 0$, we have

$$\mathbb{P}(\|C_w^e\|_2 \geq t) \leq (d + |\mathcal{Y}|) \exp\left(-\frac{t^2}{2\sigma^2 u}\right) \leq 2u \exp\left(-\frac{t^2}{2\sigma^2 u}\right). \quad (35)$$

Choosing $t = \sigma\sqrt{2u \ln(4u)}$ yields $\mathbb{P}(\|C_w^e\|_2 \leq \sigma\sqrt{2u \ln(4u)}) \geq \frac{1}{2}$. In the remainder, we work on this setting which holds with probability at least $1/2$. Let $\mathbf{h}_G = (R \circ U)(\mathbf{A}, \mathbf{X}) \in \mathbb{R}^d$ be the graph-level representation. Then, we have

$$\begin{aligned} f^e(\mathbf{A}, \mathbf{X}) - f(\mathbf{A}, \mathbf{X}) &= (C_w + C_w^e)\mathbf{h}_G - C_w\mathbf{h}_G = C_w^e\mathbf{h}_G. \\ \mathbb{E}\|f^e(\mathbf{A}, \mathbf{X}) - f(\mathbf{A}, \mathbf{X})\|_2^2 &= \mathbb{E}\|C_w^e\mathbf{h}_G\|_2^2 \leq \mathbb{E}\|C_w^e\|_2^2 \cdot \mathbb{E}\|\mathbf{h}_G\|_2^2. \end{aligned} \quad (36)$$

Moreover, $\mathbb{E}\|\mathbf{h}_G\|_2^2 = \text{tr}(\mathbb{E}[\mathbf{h}_G\mathbf{h}_G^\top]) = \text{tr}(\text{Cov}[\mathbf{h}_G] + \mathbb{E}[\mathbf{h}_G]\mathbb{E}[\mathbf{h}_G]^\top)$. Assuming the representations are centered, i.e., $\mathbb{E}[\mathbf{h}_G] = 0$, we obtain $\mathbb{E}\|\mathbf{h}_G\|_2^2 = \text{tr}(\text{Cov}[\mathbf{h}_G])$. By the law of total covariance,

$$\text{Cov}[\mathbf{h}_G] = \mathbb{E}[\text{Cov}[\mathbf{h}_G | y]] + \text{Cov}[\mathbb{E}[\mathbf{h}_G | y]]. \quad (37)$$

Under the additional standing assumption that classes occur with equal probability $1/|\mathcal{Y}|$, we have

$$\text{tr}(\mathbb{E}[\text{Cov}[\mathbf{h}_G | y]]) = \text{tr}\left(\frac{1}{|\mathcal{Y}|} \sum_{y \in \mathcal{Y}} \text{Cov}[\mathbf{h}_G | y]\right). \quad (38)$$

Furthermore, let $\boldsymbol{\mu}_y = \mathbb{E}[\mathbf{h}_G | y]$ and I_y is a subset of \mathcal{S} that graph samples belonging to the class y , the above term can be written as

$$\begin{aligned} \text{tr}\left(\frac{1}{|\mathcal{Y}|} \sum_{y \in \mathcal{Y}} \text{Cov}[\mathbf{h}_G | y]\right) &= \frac{1}{|\mathcal{Y}|} \sum_{y \in \mathcal{Y}} \frac{1}{|I_y|} \sum_{G \in I_y} \|\mathbf{h}_G - \boldsymbol{\mu}_y\|_2^2, \\ \text{tr}(\text{Cov}(\mathbb{E}[\mathbf{h}_G | y])) &= \text{tr}\left(\frac{1}{2|\mathcal{Y}|^2} \sum_{y \neq y'} (\boldsymbol{\mu}_y - \boldsymbol{\mu}_{y'}) (\boldsymbol{\mu}_y - \boldsymbol{\mu}_{y'})^\top\right). \end{aligned} \quad (39)$$

Using the margin condition encoded by $\tilde{\rho}$ and the head norm $\|C\|_2$, we upper bound this term by

$$\text{tr}(\text{Cov}(\mathbb{E}[\mathbf{h}_G | y])) \leq \frac{(|\mathcal{Y}| - 1)\tilde{\rho}^2}{|\mathcal{Y}|\|C\|_2^2}. \quad (40)$$

Combining these above and using the spectral-norm event $\|C_w^e\|_2 \leq \sigma\sqrt{2u \ln(4u)}$ (it holds with probability $\geq 1/2$) and let $\text{Var}_{\text{icv}}(\mathcal{S}, \mathcal{Y}) = \frac{1}{|\mathcal{Y}|} \sum_{y \in \mathcal{Y}} \frac{1}{|I_y|} \sum_{G \in I_y} \|\mathbf{h}_G - \boldsymbol{\mu}_y\|_2^2$, we obtain

$$\mathbb{E}\|f^e(\mathbf{A}, \mathbf{X}) - f(\mathbf{A}, \mathbf{X})\|_2^2 \leq \sigma^2 2u \ln(4u) \left(\text{Var}_{\text{icv}}(\mathcal{S}, \mathcal{Y}) + \frac{\tilde{\rho}^2}{\|C\|_2^2} \right). \quad (41)$$

To meet the stability requirement in Lemma A.1, we can choose the value of σ , enabling the right-hand side to equal $\tilde{\rho}^2$:

$$\sigma^2 2u \ln(4u) \left(\text{Var}_{\text{icv}}(\mathcal{S}, \mathcal{Y}) + \frac{\tilde{\rho}^2}{\|C\|_2^2} \right) = \tilde{\rho}^2, \quad (42)$$

which yields $\sigma^2 = \frac{\tilde{\rho}^2}{2u \ln(4u) \left(\text{Var}_{\text{icv}}(\mathcal{S}, \mathcal{Y}) + \frac{\tilde{\rho}^2}{\|C\|_2^2} \right)}$. We take a Gaussian prior P whose scale parameter matches the perturbation variance σ^2 . With the above choice of σ , the corresponding KL divergence term is bounded by

$$\text{KL}(w + u \| P) \leq \frac{u \ln(4u) \left(\text{Var}_{\text{icv}}(\mathcal{S}, \mathcal{Y}) + \frac{\tilde{\rho}^2}{\|C\|_2^2} \right)}{\tilde{\rho}^2}. \quad (43)$$

Substituting Eq.(43) into Lemma A.1, we finish the proof. \square

A.2 Proof of Theorem 4.2

PROOF. Fix a class y with index set I_y and $|I_y| \geq 1$. For each sample $G \in I_y$, we denote the cross-entropy gradients by

$$\mathbf{g}_G = \nabla_{\mathbf{h}_G} \mathcal{L}_{\text{ce}}, \quad \bar{\mathbf{g}}_y = \frac{1}{|I_y|} \sum_{G \in I_y} \mathbf{g}_G. \quad (44)$$

We define $S_y = \sum_{G \in I_y} w_G \|\mathbf{h}_G - \boldsymbol{\mu}_y\|_2^2$, so $\mathcal{L}_{\text{icv}} = \sum_y \frac{1}{|I_y|} S_y$. By computing $\nabla_{\mathbf{h}_G} S_y$ for a fixed class y and the graph sample $G \in I_y$, we obtain

$$\begin{aligned} \nabla_{\mathbf{h}_G} \mathcal{L}_{\text{icv}} &= \frac{2}{|I_y|} \left[w_G (\mathbf{h}_G - \boldsymbol{\mu}_y) - s_y \right], \\ s_y &= \frac{1}{|I_y|} \sum_{G' \in I_y} w_{G'} (\mathbf{h}_{G'} - \boldsymbol{\mu}_y) = \frac{1}{|I_y|} \sum_{G' \in I_y} w_{G'} \mathbf{d}_{G'}. \end{aligned} \quad (45)$$

With the learning rate $\eta > 0$, the gradient update on $\mathcal{L}_{\text{total}}$ yields

$$\mathbf{h}_G^+ = \mathbf{h}_G - \eta \nabla_{\mathbf{h}_G} \mathcal{L}_{\text{total}} = \mathbf{h}_G - \eta \mathbf{g}_G - \frac{2\lambda_r \eta}{|I_y|} (w_G \mathbf{d}_G - s_y), \quad (46)$$

Averaging Eq.(46) over $G \in I_y$ and using $\sum_{G \in I_y} \mathbf{d}_G = 0$, we have

$$\boldsymbol{\mu}_y^+ = \frac{1}{|I_y|} \sum_{G \in I_y} \mathbf{h}_G^+ = \boldsymbol{\mu}_y - \eta \bar{\mathbf{g}}_y. \quad (47)$$

Subtracting Eq.(47) from Eq.(46) yields the deviation recursion:

$$\mathbf{d}_G^+ = \mathbf{h}_G^+ - \boldsymbol{\mu}_y^+ = \left(1 - \frac{2\lambda_r \eta}{|I_y|} w_G\right) \mathbf{d}_G - \eta (\mathbf{g}_G - \bar{\mathbf{g}}_y) + \frac{2\lambda_r \eta}{|I_y|} s_y. \quad (48)$$

We define the intra-class variance and introduce some notations:

$$M_y = \frac{1}{|I_y|} \sum_{G \in I_y} \|\mathbf{d}_G\|_2^2, \quad M_y^+ = \frac{1}{|I_y|} \sum_{G \in I_y} \|\mathbf{d}_G^+\|_2^2, \quad M := \sum_y M_y, \quad (49)$$

$$a_G = 1 - \frac{2\lambda_r \eta}{|I_y|} w_G, \quad \mathbf{u}_G = a_G \mathbf{d}_G, \quad \mathbf{v}_G = -\eta (\mathbf{g}_G - \bar{\mathbf{g}}_y) + \frac{2\lambda_r \eta}{|I_y|} s_y, \quad (50)$$

so that Eq.(48) becomes $\mathbf{d}_G^+ = \mathbf{u}_G + \mathbf{v}_G$. The inequality $\|\mathbf{u} + \mathbf{v}\|_2^2 \leq \|\mathbf{u}\|_2^2 + \|\mathbf{v}\|_2^2$ gives

$$M_y^+ \leq \frac{1}{|I_y|} \sum_{G \in I_y} a_G^2 \|\mathbf{d}_G\|_2^2 + \frac{1}{|I_y|} \sum_{G \in I_y} \|\mathbf{v}_G\|_2^2. \quad (51)$$

Since $w_G \in [\frac{1}{|\mathcal{Y}|}, 1]$, we have

$$a_r^2 = \left(1 - \frac{2\lambda_r \eta}{|I_y|} w_G\right)^2 \leq 1 - \frac{4\lambda_r \eta}{|\mathcal{Y}||I_y|} + \frac{4\lambda_r^2 \eta^2}{|I_y|^2}. \quad (52)$$

Substituting into the first term of Eq.(51) yields

$$\frac{1}{|I_y|} \sum_{G \in I_y} a_r^2 \|\mathbf{d}_G\|_2^2 \leq \left(1 - \frac{4\lambda_r \eta}{|\mathcal{Y}||I_y|} + \frac{4\lambda_r^2 \eta^2}{|I_y|^2}\right) M_y. \quad (53)$$

We then show how to bound $\frac{1}{|I_y|} \sum_{G \in I_y} \|\mathbf{v}_G\|_2^2$. First, we have

$$\frac{1}{|I_y|} \sum_{G \in I_y} \|\eta (\mathbf{g}_G - \bar{\mathbf{g}}_y)\|_2^2 \leq 4\eta^2 \max_G \|\mathbf{g}_G\|_2^2. \quad (54)$$

By Cauchy–Schwarz inequality, we have

$$\|s_y\|_2 \leq \frac{1}{|I_y|} \sum_{G \in I_y} w_G \|\mathbf{d}_G\|_2 \leq \frac{1}{|I_y|} \sum_{G \in I_y} \|\mathbf{d}_G\|_2 \leq \sqrt{M_y}, \quad (55)$$

and therefore $\left\| \frac{2\lambda_r \eta}{|I_y|} s_y \right\|_2^2 \leq \frac{4\lambda_r^2 \eta^2}{|I_y|^2} M_y$.

Using $\|a + b\|_2^2 \leq 2\|a\|_2^2 + 2\|b\|_2^2$, we obtain

$$\frac{1}{|I_y|} \sum_{G \in I_y} \|\mathbf{v}_G\|_2^2 \leq 8\eta^2 \max_G \|\mathbf{g}_G\|_2^2 + \frac{8\lambda_r^2 \eta^2}{|I_y|^2} M_y. \quad (56)$$

Substituting Eq.(53) and Eq.(56) into Eq.(51), we conclude

$$M_y^+ \leq \left(1 - \frac{4\lambda_r \eta}{|\mathcal{Y}||I_y|} + \frac{4\lambda_r^2 \eta^2}{|I_y|^2}\right) M_y + 8\eta^2 \max_G \|\mathbf{g}_G\|_2^2 + \frac{8\lambda_r^2 \eta^2}{|I_y|^2} M_y \quad (57)$$

Summing over all classes, we obtain the global one-step recursion:

$$M^+ \leq \left(1 - \frac{4\lambda_r \eta}{|\mathcal{Y}| \min_y |I_y|} + \frac{12\lambda_r^2 \eta^2}{\max_y |I_y|^2}\right) M + 8 \max_G \|\mathbf{g}_G\|_2^2 \eta^2. \quad (58)$$

If η is a constant and $0 < \eta < \min\left\{\frac{\max_y |I_y|^2}{6k\lambda_r \min_y |I_y|}, \frac{|\mathcal{Y}| \min_y |I_y|}{2\lambda_r}\right\}$, then $1 - \frac{4\lambda_r \eta}{|\mathcal{Y}| \min_y |I_y|} + \frac{12\lambda_r^2 \eta^2}{\max_y |I_y|^2} \leq 1 - \frac{2\lambda_r}{|\mathcal{Y}| \min_y |I_y|} \eta = \rho_\eta \in (0, 1)$, and iterating (58) yields

$$M^{(t)} \leq \rho_\eta^t M^{(0)} + \frac{8\eta^2}{1 - \rho_\eta} \max_{G,t} \|\mathbf{g}_G^{(t)}\|_2^2 = \rho_\eta^t M^{(0)} + \mathcal{O}(\eta) \max_{G,t} \|\mathbf{g}_G^{(t)}\|_2^2, \quad (59)$$

which proves geometric convergence to an $\mathcal{O}(\eta)$ neighborhood. \square